

Source Characteristics of the 22 January 2003 $M_w = 7.5$ Tecomán, Mexico, Earthquake: New Insights

LUIS QUINTANAR,¹ HÉCTOR E. RODRÍGUEZ-LOZOYA,² ROBERTO ORTEGA,³ JUAN M. GÓMEZ-GONZÁLEZ,⁴
TONATIUH DOMÍNGUEZ,⁵ CLARA JAVIER,⁶ LEONARDO ALCÁNTARA,⁷ and CECILIO J. REBOLLAR⁸

Abstract—Aftershock locations, source parameters and slip distribution in the coupling zone between the overriding North American and subducted Rivera and Cocos plates were calculated for the 22 January 2003 Tecomán earthquake. Aftershock locations lie north of the El Gordo Graben with a northwest-southeast trend along the coast and superimposed on the rupture areas of the 1932 ($M_w = 8.2$) and 1995 ($M_w = 8.0$) earthquakes. The Tecomán earthquake ruptured the northwest sector of the Colima gap, however, half of the gap remains unbroken. The aftershock area has a rectangular shape of 42 ± 2 by 56 ± 2 km with a shallow dip of roughly 12° of the Wadati-Benioff zone. Fault geometry calculated with the Nábělek (1984) inversion procedure is: (strike, dip, rake) = (277° , 27° , 78°). From the teleseismic body wave spectra and assuming a circular fault model, we estimated source duration of 20 ± 2 s, a stress drop of 5.4 ± 2.5 MPa and a seismic moment of $2.7 \pm .7 \times 10^{20}$ Nm. The spatial slip distribution on the fault plane was estimated using new additional near field strong motion data (54 km from the epicenter). We confirm their main conclusions, however we found four zones of seismic moment release clearly separated. One of them, not well defined before, is located toward the coast down dip. This observation is the result of adding new data in the inversion. We calculated a maximum slip of 3.2 m, a source duration of 30 s and a seismic moment of 1.88×10^{20} Nm.

Key words: Rupture process, focal mechanism inversion, waveform modeling.

C. J. Rebollar: deceased September 2006.

¹ Instituto de Geofísica, Universidad Nacional Autónoma de México, México D.F., Mexico. E-mail: luisq@ocean.geofisica.unam.mx

² Facultad de Arquitectura, Facultad de Ingeniería Civil, Universidad Autónoma de Sinaloa, Culiacán, Mexico.

³ Centro de Investigación Científica y de Educación Superior de Ensenada, Unidad La Paz, La Paz, Mexico.

⁴ Centro de Geociencias, Universidad Nacional Autónoma de México, Juriquila, Querétaro, Mexico.

⁵ Observatorio Vulcanológico de Colima, Universidad de Colima, Colima, Mexico.

⁶ Comisión Federal de Electricidad, Gerencia de Estudios de Ingeniería Civil, Guadalajara, Mexico.

⁷ Instituto de Ingeniería, Universidad Nacional Autónoma de México, México D.F., Mexico.

⁸ Centro de Investigación Científica y de Educación Superior de Ensenada, Ensenada, Mexico.

1. Introduction

The subduction zone that encompasses the Mexican states of Jalisco and Colima, (Fig. 1a) has produced the largest earthquakes in Mexico. Offshore of the state of Colima, the Rivera, Cocos and North America plates interact (Fig. 1a). In this seismogenic area the 1932, magnitude 8.2, Jalisco earthquake occurred, the largest earthquake in Mexico in recent documented seismological history (SINGH *et al.*, 1985; SUÁREZ *et al.*, 1994). The 22 January 2003 ($M_w = 7.5$) Tecomán earthquake occurred between the rupture areas of the 9 October 1995 ($M_w = 8.0$) Colima–Jalisco earthquake and the 30 January 1973 ($M_w = 7.6$) Colima earthquake (see Fig. 1b) (REYES *et al.*, 1979; PACHECO *et al.*, 1997). The Tecomán earthquake was located by the University of Colima at 18.625° N, 104.125° W, at a depth of 10 km and with an origin time of 02 h 06 min and 35.0 s. This earthquake badly damaged the state of Colima, damaging and collapsing adobe houses, unreinforced masonry structures and construction in poorly consolidated fills, and producing landslides. Liquefaction was also observed in the Manzanillo port.

A preliminary study of the Tecomán earthquake was carried out by SINGH *et al.*, (2003). They reported a preliminary aftershock area, gross source characteristics, attenuation of strong motion data and an isoseismal map. NÚÑEZ-CORNU *et al.*, (2004) reported the aftershock locations of the first 72 h after the main shock and found that the seismic activity was mainly in the continental plate along two NW–SE trending zones. YAGI *et al.*, (2004) estimated the spatial and temporal slip over the fault plane of the Tecomán earthquake, inverting regional strong motion data as well as teleseismic body-

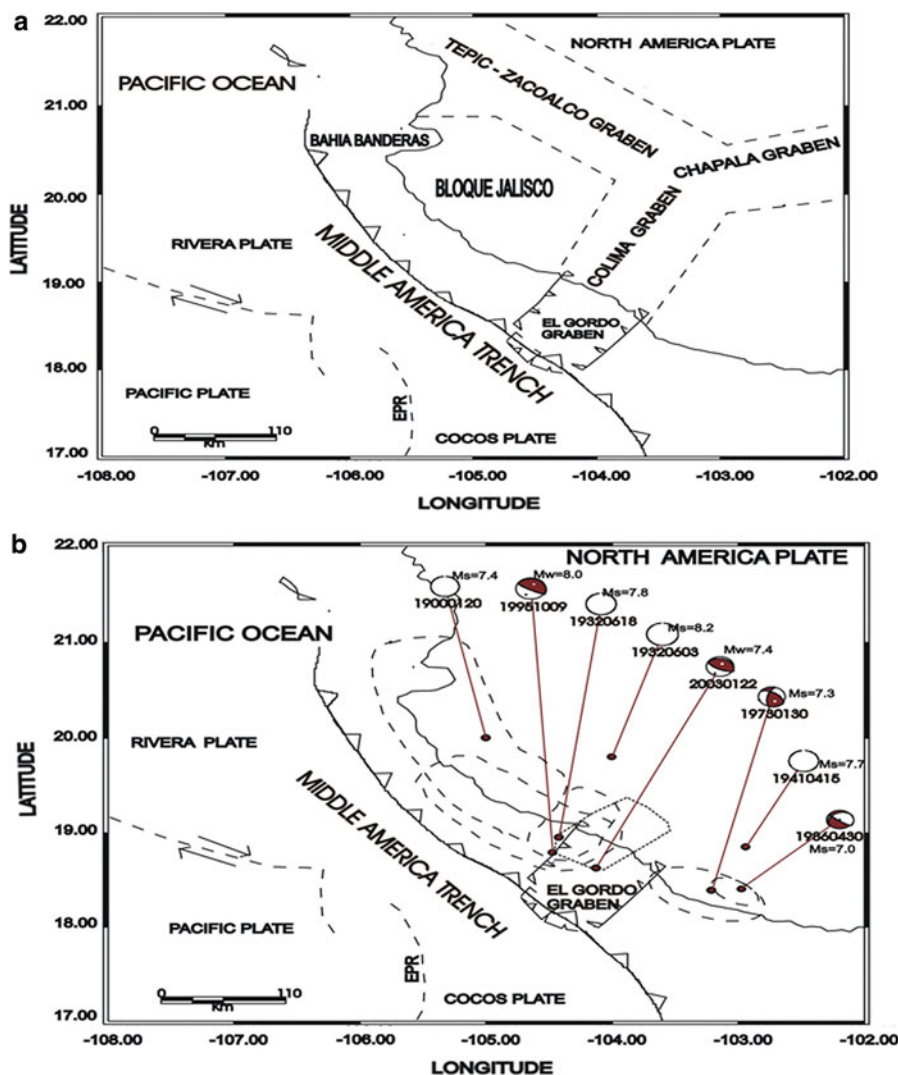


Figure 1

a Tectonic framework of the Colima–Jalisco region. **b** Location of earthquakes >7 that have occurred in the Colima–Jalisco region. Light dashed lines show the rupture area of the 1932 ($M_w = 8.2$) earthquake (SINGH *et al.*, 1985). Heavy dashed line is the rupture area of the 1995 ($M_w = 8.0$) earthquake (PACHECO *et al.*, 1997). Also shown are the aftershock areas of the 1973 ($M_w = 7.3$) and 1986 (1980) ($M_w = 7.0$) earthquakes. Continuous line is the aftershock area of the 2003 Tecomán earthquake. Available focal mechanisms are also shown. EPR east Pacific rise

waves. The closest near field strong motion station they used was located 138 km from the epicenter. In the inversion process they used a slightly modified fault plane geometry reported by the Harvard CMT solution. They found three stages in the rupture process: (1) the rupture nucleated near the hypocenter, (2) the first asperity, centering about 15 km southwest from the epicenter, was broken and (3)

the rupture propagated to the northeast and the second asperity was broken.

In the present study, we revise the aftershock area employing newly calculated hypocenters using arrival times recorded at the Colima seismic network (Red Sismica de Colima, RESCO) and nine portable seismic stations deployed by CICESE (Centro de Investigación Científica y de Educación Superior de

Ensenada). We found that the aftershocks lay mainly along the coupling zone of the plates and inside the subducted slab. We also calculated the stress drops and source duration of the main event with the spectral analysis of body P-waves recorded by broadband seismic stations located at teleseismic distances, following BEZZEGHOUD *et al.*, (1989), assuming a circular fault model (BRUNE, 1970). In this study of the Tecomán event, we used near field strong motion waveforms recorded at the Manzanillo power plant located 54 km from the epicenter; data which have not been previously used. We combined this strong-motion data with the data used by YAGI *et al.*, (2004) to obtain the slip on the fault plane and to analyze how much the additional near field data modified the previously reported slip distribution on the fault.

2. Tectonic and Historical Seismicity

West of the Mexican Volcanic Belt lies the junction of the North American, Pacific and Cocos plates. The Rivera and Cocos plates subduct at a rate of 5 cm/year (KOSTOGLODOV and BANDY, 1995) beneath North America, below the states of Colima and Jalisco. In the North American plate a tectonic block called the Jalisco Block (JB) is limited to the west by the Rivera plate, to the south and southeast by El Gordo-Colima graben and toward the east and northeast by the Chapala and Tepic-Zacoalco Grabens (Fig. 1a). Major seismic activity is due mainly to the collision of the Cocos–Rivera plates with the North American plate and occurs in the coupling zone. Depths of major underthrusting earthquakes range from 10 to 32 km. According to PARDO and SUÁREZ, (1995) seismic activity starts to decrease toward Bahía Banderas, located northwest of the JB, reaching depths on the order of 100 km (see Fig. 1a). The Wadati-Benioff zone increases its dip from $\sim 25^\circ$ in the southeast to 46° toward Bahía Banderas. Table 1 and Fig. 1b shows the location, rupture areas, and seismic moments of earthquakes of magnitude >7 that have occurred in this region.

3. Data Recording Systems

The Volcanic Observatory of the University of Colima maintains a short period and broadband telemetered network of seismic stations around the Colima volcano and along the Colima coast. This network, called Red Sísmica de Colima (RESCO), consists of 11 short period seismometers and 2 broadband CMG-40T Guralp seismometers. Data are continuously recorded and sent by radio links to the University of Colima where they are stored and analyzed. RESCO stations, which record at 100 samples per second, recorded the Tecomán event and all its aftershocks. A week after the occurrence of the main event, CICESE deployed a portable seismic network of nine short period GBV seismic recorders with a natural period of 4.5 Hz, as well as, a broadband Guralp CMG-40T seismometer that recorded continuously at 100 samples per second with a CMG-SAM2 acquisition module. All GBV seismic stations recorded in a triggered mode at 100 samples per second. Figure 2a shows the location of the seismic stations and Fig. 2b the location of the strong motion stations.

4. Aftershock locations and dip of the Wadati-Benioff zone

Aftershock locations were determined with the HYPO71 program using a one-dimensional crustal structure (shown in Table 2) routinely used by RESCO. Due to the occurrence of the aftershocks toward the ocean and the location of the seismic stations, azimuthal coverage is poor. We located aftershocks that included P and S wave arrival times at seismic stations located along the coast in order to better constrain focal depths. Figure 3 shows an example of the traces of an aftershock recorded in 19 seismic stations. Impulsive P wave arrivals as well as the onsets of S waves can be seen. We started locating aftershocks with initial fixed depths in the range from 10 to 50 km with steps of 5 km. From the HYPO71 outputs we chose those locations with average root mean square error of time residuals (rms) of 0.6 ± 0.3 s, average standard error of the epicenter

Table 1

Location and seismic moments of earthquakes of magnitude >7 that have occurred in the study region

Date	H:min.	Lat.	Lon.	Seismic moment (Nm)	Magnitude (Ms ^c , M _w ^a)	Depth (Km)
19000120	06:33	20.00	-105.00	-	7.4 ^c	-
19320603	10:36	19.80	-104.00	9.10×10^{20}	8.2 ^c , 8.0 ^a	16.0
19320618	10:12	18.95	-104.42	7.3×10^{20}	7.8 ^c	16.0
19410415	19:09	18.85	-102.94	-	7.7	-
19730130	21:01:00	18.39	-103.21	3.0×10^{20}	7.3 ^{bc}	32.0
19950910	15:35:53.0	19.05	-104.20	9.1×10^{20}	8.0	17.0
20030122	02:06:33.8	18.625	-104.125	1.60×10^{20}	7.4 ^a	10.0

^a RESCO^b Reyes et al. (1979)^c Pacheco and Sykes (1992)

(ERH) of 3.3 ± 1.8 km and average standard error of the focal depth (ERZ) of 3.1 ± 2.8 . The errors are plus or minus one standard deviation. Ninety aftershocks fulfilled the above mentioned error criteria. Local magnitudes of the located events range from 2 to 3.

Figure 4 shows the location of the aftershocks in a plan view, from which it can be seen that the activity lies north of El Gordo Graben and that the aftershock area encompasses parts of the rupture areas of the 1932 and 1995 events. The area between the limits of the rupture areas of the 1995 and the 1973 earthquakes is the Colima seismic gap. The northwest area of this gap ruptured with the Tecomán earthquake. Toward the southeast, roughly half of the gap remains unbroken.

Figure 5 shows vertical cross-sections of aftershocks projected perpendicular and parallel to the middle America trench (MAT) as well as the projection of the P-axes of the Tecomán event and two of the largest aftershocks of magnitudes 5.7 and 5.3. Also shown is the projection of the 1995 $M_w = 8.0$ Colima–Jalisco event. The hypocenter (where the rupture started) of the Tecomán event lies within the coupling zone between the subducted Cocos–Rivera plates and the overriding North American plate. The boundary between the subducted slab and the continental crust was taken from cross section ‘K’ of PARDO and SUÁREZ, (1995). The source mechanisms of the main event and two of the largest aftershocks were all thrust events. The projections of the P-axes of the main event and the largest aftershocks show that these compressional axes are oblique to the

interface of the overriding and subducted slab. One of the aftershocks (focal depth of 5 km) was an interplate event, while the second large aftershock (focal depth of 14 km) was an intraplate event. Fault plane solutions of the largest aftershocks were taken from SINGH *et al.*, (2003). Using the obtained aftershocks’ depth, we inferred that the Wadati–Benioff zone in the coupling area has a dip of 12° up to a distance of 85 km from the trench (see Fig. 5a); beyond that point the Wadati–Benioff increases to a dip of 50° according to PARDO and SUÁREZ, (1995). Most of the aftershock activity of the 2003 Tecomán sequence occurred within the subducted plate and along the overriding North American plate. The thick line on Fig. 5a depicts our interpretation of the coupling zone. On the other hand, Fig. 5b shows a cross-section parallel to the MAT, from this figure we roughly calculated a rupture area of 44 by 58 km. Aftershock depths range from 5 to 38 km.

5. Focal Mechanism Determination

To obtain the fault geometry we carried out a waveform inversion with the point source approximation using P and SH recorded at teleseismic distances following Nábělek (1984). We used data from stations at epicentral distances between $30^\circ < \Delta_P < 91^\circ$ and $35^\circ < \Delta_{SH} < 83^\circ$ for P and SH waves, respectively. Various corrections were included for a direct comparison between synthetic and observed seismograms. Such corrections take care of the geometrical spreading, the instrumental response,

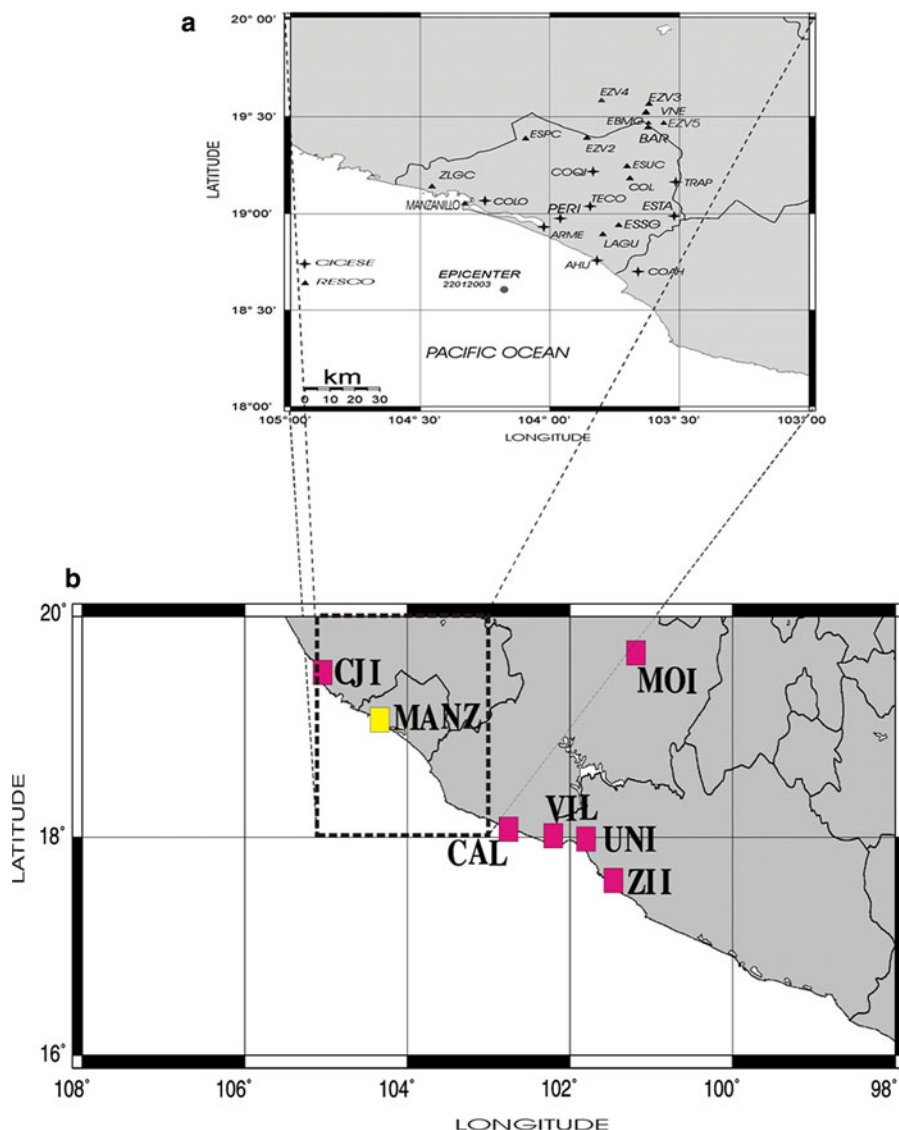


Figure 2

a Location of RESCO (full triangles) seismic stations and CICESE (crosses) portable stations. **b** Map showing the strong motion instruments from UNAM (full squares). Empty square shows the location of the Manzanillo strong-motion recorder located in the Manzanillo power plant

Table 2

Velocity model used for aftershocks location

P-wave velocity (km/s)	Layer depth (km)
1.7	0.0
2.7	2.0
3.6	3.0
4.6	4.0
5.7	6.0
6.0	12.0
7.4	18.0
7.8	35.0

the amplitude and phase distortions which are due to a layered crust. The anelastic attenuation of the Earth (FUTTERMAN, 1962) is responsible for these distortions. To correct for it, we used a frequency independent Q average seismic quality factor along the ray, which is assumed a constant value of $t^* = T/Q$, where T is the ray travel time. Here we used $t^* = 1.0$ and 4.0 s for P and SH waves, respectively.

The effects of the structure below the receiver were neglected and we consider the response to be

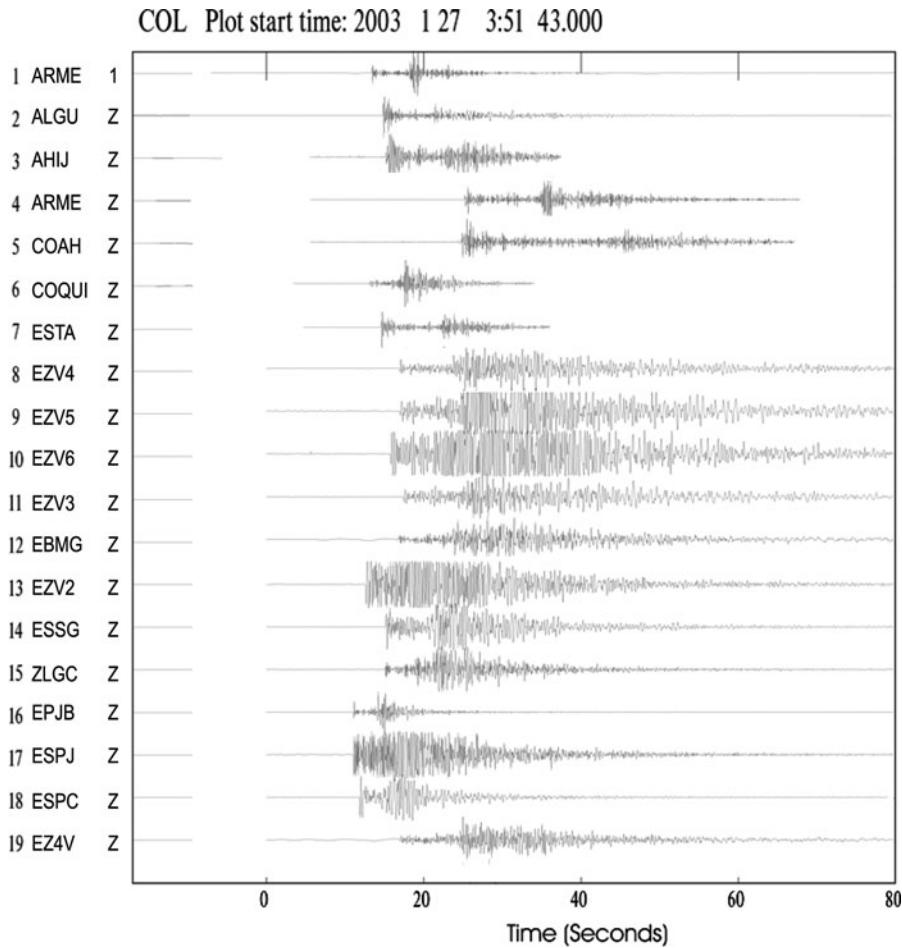


Figure 3

Example of an aftershock recorded by the 19 seismic stations (only the vertical component is shown). Impulsive P -wave arrivals and clear onsets of some S waves can be seen; traces are normalized to one. Names of the seismic stations are indicated

controlled mostly by the source radiation pattern at the near source structure. Green's functions around the source were computed and a stratified velocity model was assumed (Table 3) based on the crustal structure of REYES *et al.*, (1979). A simple half-space model at the receiver was used ($V_p = 6.0$ km/s, $V_s = 3.46$ km/s, $\rho = 2.8$ g/cm³ and a Poisson ratio of 0.25). Seismograms were band-pass filtered using a third-order Butterworth filter from 0.01 to 0.4 Hz and corrected for instrument responses. Sixty seconds of vertical P and transverse SH wave displacements were obtained through integration of the velocity records. Good station coverage made it possible to obtain the fault geometry. The event was modeled using 7 overlapping triangles with 2.5 s of rise time.

We obtained the following mechanism: (strike, dip, rake) = (277°, 27°, 78°), and a scalar seismic moment of 1.3×10^{20} Nm and a apparent source time function of 20 s. By searching for the best centroid depth, the residual error minimized at 25 km, which is similar to that reported by YAGI *et al.*, (2004). Waveform fitting was good even for SH waves, which are usually difficult to fit. Figure 6 shows a comparison between observed and synthetic waveforms and the apparent source time function. P -wave fitting around the fault plane is reasonably good. Southward stations, in the dilatation quadrant close to the sub-vertical nodal plane (PTCN and RPN), constrained the strike of the south dipping plane. This is important because most of the stations

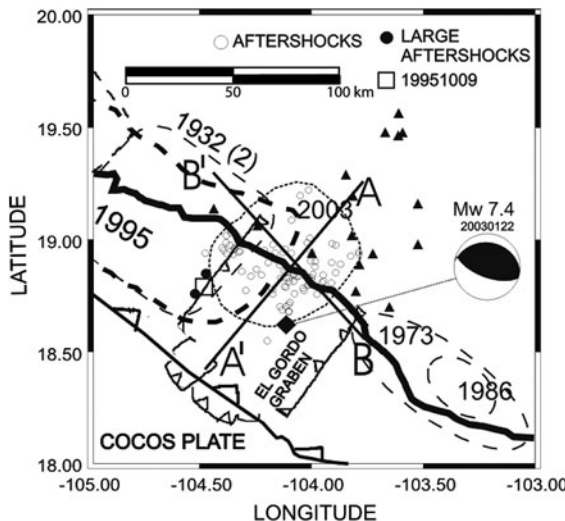


Figure 4

Map showing our best aftershock locations (empty circles). Large full square shows the epicenter location of the Tecomán earthquake. Its fault plane solution is also shown. Large empty square shows the epicenter location of the Colima–Jalisco earthquake of 1995 ($M_w = 8.0$). Profiles AA' and BB' are cross sections onto which aftershocks were projected shown in Fig. 5. Triangles show the locations of seismic stations

were distributed into the compression quadrant. A similar good quality fitting was found for SH-waves; stations PTCN, DSB, HRV, and MTE fixed one of the nodal planes. The NÁBĚLEK, (1984) point source waveform fitting was good to constrain the fault geometry, however, it clearly underestimated the seismic moment and the apparent source time function (also shown in the middle). Finite two-dimension source inversion (described later) showed that some patches of slip are detected by near field stations which raised the scalar moment, and that displacement could not be detected by the point source approximation at teleseismic distances, especially those displacements near the edge of the fault plane.

6. Static Stress Drop Estimate

We calculated the P-wave spectra of the Tecomán earthquake recorded at broadband stations at teleseismic distances. We used IRIS and GEOSCOPE seismic stations in order to estimate source parameters. P-wave windows of 70 s, which included 10 s of noise prior to the P-wave arrival and 60 s of the P

wave trains, were used in the spectral analysis. No filter was applied to the P wave trains. After calculating the fast Fourier transform, we estimated the seismic moment rate at each seismic station by:

$$\frac{\partial}{\partial t}M(f) = \frac{4\pi\rho\alpha^3a}{g(\Delta, h)C(i)} \left[\frac{Q(f)W(f)}{I(f)S_{\text{rad}}(f)} \right] \quad (1)$$

where ρ is the density at the source, α is the P wave velocity at the source, a is the radius of the earth, $C(i)$ is the surface amplification at the i th seismic station, $Q(f)$ is the seismic attenuation, $g(\Delta, h)$ is the geometrical dispersion, $W(f)$ is the spectral displacement, $I(f)$ is the instrument response and $S_{\text{rad}}(f)$ is the radiation pattern as a function of frequency of the P, pP and sP waves.

Data was corrected for instrument response, attenuation, and radiation pattern. Following BEZZEGHOUD *et al.*, (1989), we substituted the effective radiation pattern $S_{\text{rad}}(f)$ with the approximation:

$$S_{\text{rad}}(0) = R^P + R^{pP} + R^{sP} \quad (2)$$

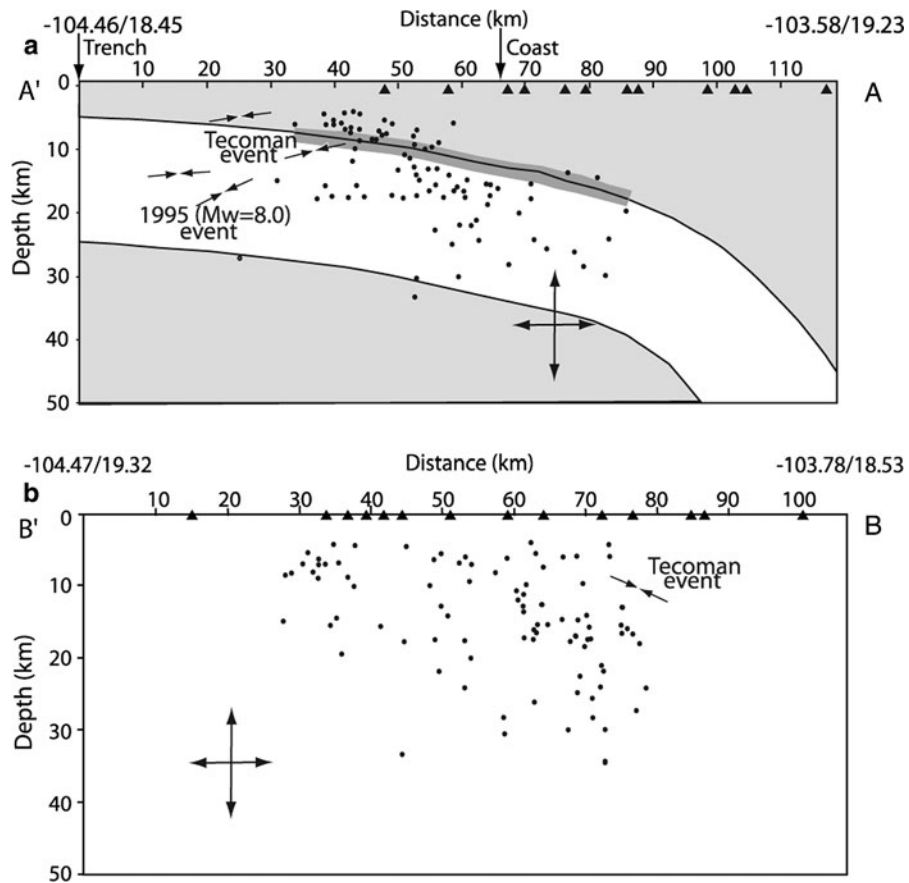
where R^P , R^{pP} , R^{sP} are the P, pP, and sP radiation pattern, respectively. The fault geometry used to calculate the radiation pattern was strike 277° , dip 27° and rake 78° . According to the hypocenter (25 km), the pP and sP wave trains arrived 7 and 10 s after the direct P wave. The attenuation operator t^* was assumed to be 1.0. The static seismic moment was calculated from the following expression:

$$M_0 = \frac{\partial}{\partial t}M(0) = \frac{4\pi\rho\alpha^3a}{g(\Delta, h)C(i)} \left[\frac{Q(0)W(0)}{I(0)S_{\text{rad}}(0)} \right] \quad (3)$$

Figure 7 shows the plot of the logarithmic mean of corrected moment rate spectra determined from the broadband displacement records of 15 P-waveforms recorded at teleseismic stations. An average seismic moment of $2.7 \pm 0.7 \times 10^{20}$ Nm ($2.7 \pm 0.7 \times 10^{27}$ dynes cm) was determined. From the spectra we obtained a corner frequency of $f = 0.05 \pm 0.005$ Hz and a slope at higher frequencies of -2.4 . The rupture time needed for the rupture to propagate along the fault is approximately:

$$T_R = \frac{L}{v_R} \quad (4)$$

Where T_R is the rupture time, which is the inverse on the corner frequency, L is the length of the fault



a Cross section of seismicity along profile AA'. **b** cross section of seismicity along profile BB'. Arrows show the projection of the P axes for the Tecomán earthquakes and two of its largest aftershocks. Subducting plate geometry was taken from PARDO and SUÁREZ, (1995). See Fig. 4 for profile locations

Table 3

Velocity model used for focal mechanism determination with teleseismic records

Thickness (km)	V_p (km/s)	V_s (km/s)	ρ (g/cm ³)
6.0	5.80	3.35	2.68
19.0	6.40	3.69	2.78
10.0	7.00	4.04	2.85
-	8.00	4.62	3.00

and v_R is the rupture velocity. Therefore, the rupture time is 20 ± 2 s and the rupture length is 66 ± 5 km, assuming a rupture velocity of $0.9V_s$ (3.3 km/s). This calculated rupture length lies within the range of the aftershock length calculated with the aftershock activity (56 ± 2 km). The stress drop on a circular fault (BRUNE, 1970) with radius R is given by

$$\Delta\sigma = \frac{7}{16} \frac{M_0}{R^3} \quad (5)$$

From the aftershock area we calculated a fault length of 56 ± 2 km so the fault radius R is 28 ± 2 km. Therefore, the stress drop of the Tecomán earthquake is 5.4 ± 2.5 MPa. This value contrasts with the higher value (~ 10 MPa) obtained by YAGI *et al.*, (2004) using regional and local records.

7. Slip Distribution Inversion

BERESNEV, (2003) argued that incorrect assumptions of crustal structure, rupture velocity, fault geometry and array geometry will generate geologic artifacts in the inversion of seismic data for slip

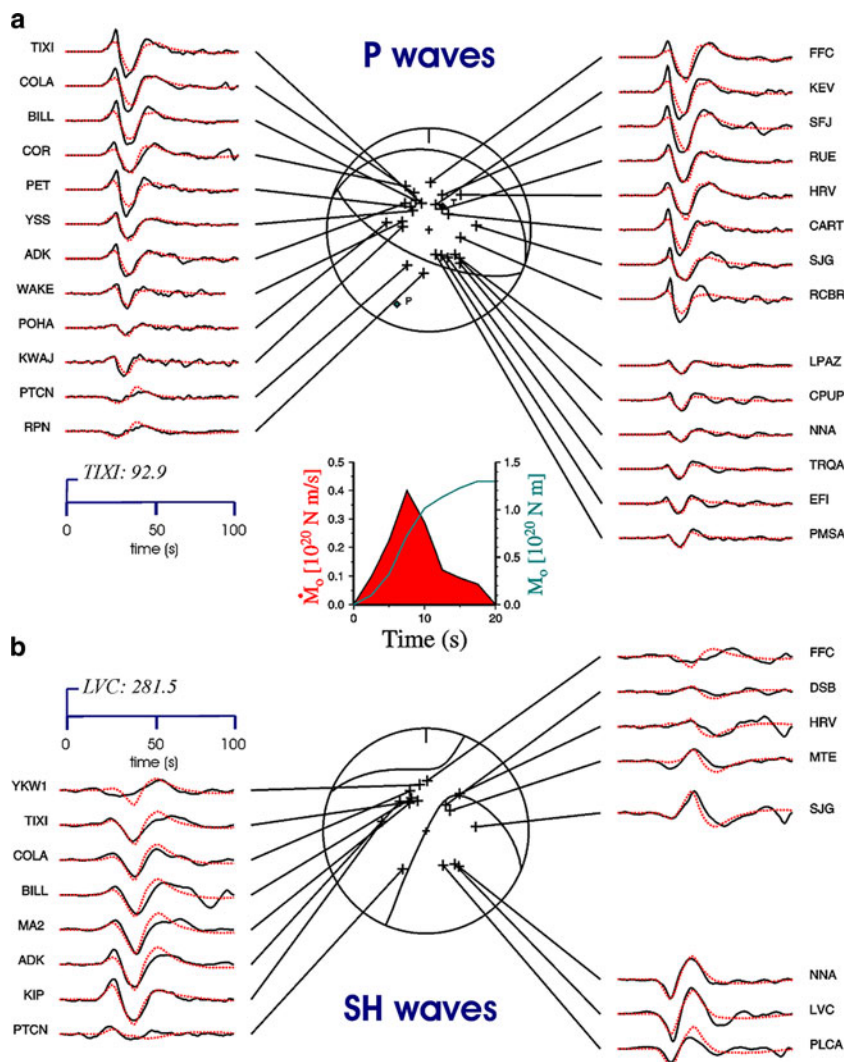


Figure 6

Point source inversion from body wave broadband data. **a** Observed P wave seismograms (black lines) and synthetics (red lines). The source time function was about 20 s and the corresponding seismic moment is 1.3×10^{20} Nm. **b** Observed SH wave seismograms (solid lines) and synthetics (dashed lines). The solution corresponds to an underthrust event with (strike, dip, rake) = (277°, 27°, 78°). The axes indicate the amplitude of the waves in microns

distribution of finite faults. On the other hand, IDE *et al.*, (2005) suggested that the quality and quantity of the data is critical to constrain the source-imaging problem. So, in line with those opinions, we decided to do the source imaging of the Tecomán event with better-constrained fault geometry and the inclusion of near field strong motion data not used previously in the study of the Tecomán event. Figure 8 shows the acceleration records of the free-field strong motion station located at the Manzanillo power plant (MNZ).

We also used data recorded at IRIS and GEOSCOPE broadband stations, strong motion records from the Servicio Sismológico Nacional (SSN) and Instituto de Ingeniería, UNAM (Fig. 2). To obtain the slip over the rupture area of the Tecomán earthquake, we used the method described by YAGI *et al.*, (1999, 2004) following the formulation of HARTZELL and HEATON, (1983), YOSHIDA (1989, 1992). The rupture process is simulated as a spatio-temporal slip distribution over the fault plane. The fault plane is divided

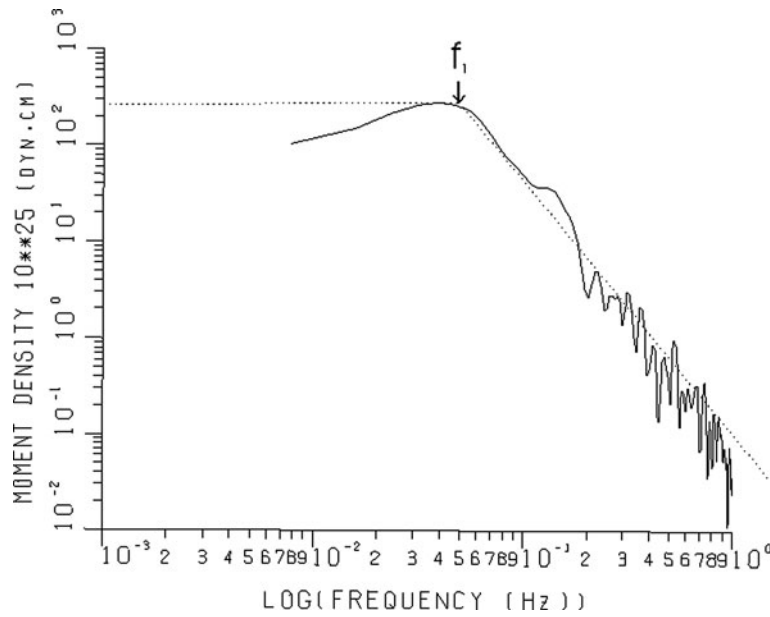


Figure 7

Average displacement spectra of teleseismic P waveforms of the Tecomán earthquake. f_c is the corner frequency and dashed lines indicate the trend at lower and higher frequencies. The slope at higher frequencies is -2.4

into $M \times N$ sub-faults with length xx and width yy . The slip-rate function at each sub-fault is described with B splines that are a series of L triangle functions with rise time τ . Slip vectors at each sub-fault are taken as vectors with components given by λ_0 , the assumed slip angle. The synthetic waveform at the j th station is given by

$$W_j^{obs}(t_i) = \sum_m \sum_n \sum_l \sum_k X_{mnlk} g_{mnkj} \times (t_i - (l-1)\tau - T_{mn}) + e,$$

where X_{mnlk} is the l th component of slip at m nth subfault at k th time step. g_{mnkj} is the Green's function from a point source at the mn -subfault, T_{mn} is the start time of the slip of the basis functions at each sub-fault and e is assumed to be a Gaussian error with variance σ . Green's functions for teleseismic body waves are calculated using the KIKUCHI and KANAMORI, (1991) method. Green's functions for near field ground motion are calculated by the discrete wave number method developed by KOHKETSU, (1985). Table 4 shows the one-dimensional elastic models used in the calculation of the Green's functions. This model is the same used by YAGI *et al.* (2004) for teleseismic

stations and has been modified lightly for strong motion stations to take into account the inclusion of the MNZ accelerograms.

In the inversion process we used the fault geometry previously calculated with the NÁBÉLEK, (1984) method given by (strike, dip, slip) = (277°, 27°, 78°). We used a larger fault area in order to follow the same procedure of YAGI *et al.*, (2004), even though the observed aftershock area is smaller. We considered a rupture area with a width of 70 km, a length of 100 km and divided the fault plane into 14 × 20 sub-faults with length of 5 km and width of 5 km. Twenty five kilometers depth of the initial front rupture was assumed. The slip-rate function on each sub-fault was expanded into a series of twelve triangles with a rise time of 2.0 s and the slip angle kept unchanged during the rupture. We used a rupture wave velocity of 3.3 km/s.

It is instructive to investigate how well the MNZ accelerogram fits with our estimated fault geometry (strike, dip, slip) = (277°, 27°, 78°) and YAGI *et al.* (2004) fault geometry (strike, dip, slip) = (300°, 20°, 93°). Figure 9 shows the comparison of the observed and synthetic accelerograms of MNZ with both fault

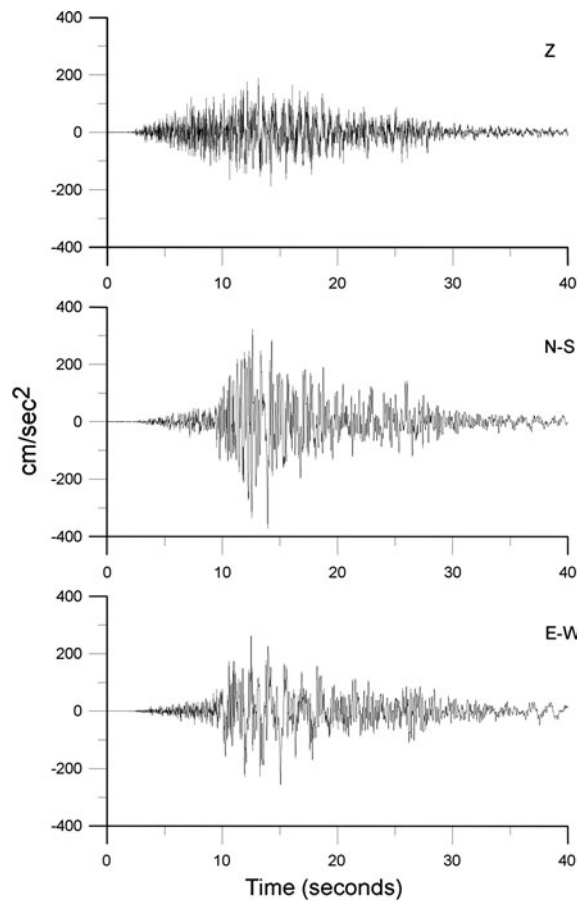


Figure 8

Acelerograms recorded in the Manzanillo (MNZ) power plant located 54 km from the epicenter

Table 4

Velocity model used for rupture process inversion with local, regional and teleseismic records

α (km/s)	β (km/s)	ρ (10^3 kg/m 3)	$Q\alpha$	$Q\beta$	Thickness (km)
<i>For teleseismic body wave</i>					
1.5	0.0	1.0			1.0
5.54	3.20	2.50			3.0
5.69	3.29	2.70			5.0
6.27	3.62	2.80			9.70
6.71	3.87	2.90			17.30
8.10	4.68	3.30			–
<i>For strong ground motion</i>					
5.69	3.37	2.70	500	250	9.0
6.27	3.54	2.80	600	300	9.7
6.71	3.82	2.90	800	400	17.3
8.00	4.53	3.25	1,200	600	–

geometries. Both geometries reproduce the main amplitudes, but our fault geometry fit better the later parts of the accelerograms of the vertical and north-south components; however both geometries failed to adequately fit the east-west component, even though our fault geometry better fit the initial onset of the first arrivals.

We performed the inversion with the near field strong motion data and the far field P-waveforms. Comparisons of the observed and synthetic waveforms, shown in Fig. 10, indicate that the fits are good. The seismic moment was 1.88×10^{20} Nm equivalent to a moment magnitude of 7.5. The source time duration lasted nearly 30 s, but the majority of the energy was released during the first 20 s, in agreement with the source time duration calculated with the teleseismic spectra and NÁBĚLEK (1984) point source inversion. Figure 11 show a horizontal projection of the slip distribution on the fault plane, which consisted mainly of the same seismic moment release found by YAGI *et al.*, (2004), however, it shows two additional zones of seismic moment release up-dip and down-dip which are barely shown in YAGI *et al.*, (2004) inversion. The maximum fault slip was 3.2 m.

8. Summary

We used data recorded by a permanent network of short period and broadband seismic stations (RESCO) and nine portable seismic stations in order determine the aftershock area of the Tecomán earthquake. Figure 4 shows our aftershock locations. A depth of 10 km for the hypocenter of the Tecomán earthquake was calculated with P-wave arrivals of local stations; we think that the rupture could have started at this depth. The depths of the main event and the aftershocks defined a shallow dip of the Wadati-Benioff zone of roughly 12° (Fig. 5). Beyond the aftershock area, the Wadati-Benioff dip increases to 50° according to PARDO and SUÁREZ, (1995), however we did not located any aftershock activity at the bend of the subducted slab. We inferred an approximate aftershock area with a rectangular shape of 42 ± 2 by 56 ± 2 km. Aftershocks were located toward the north of the location of the epicenter of the Tecomán

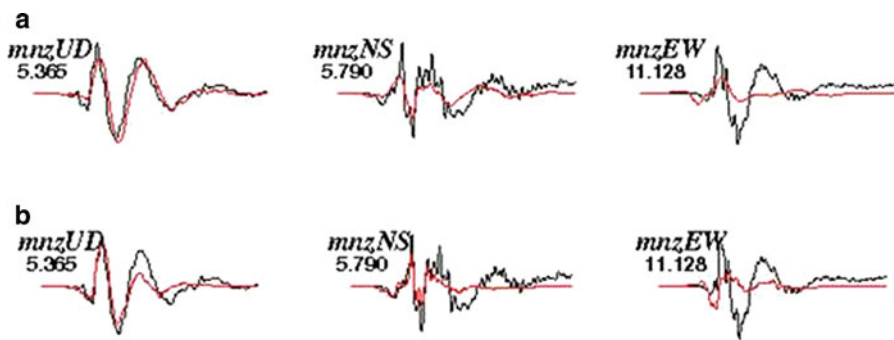


Figure 9

Comparison of modeling for the strong-motion record of MNZ station located 54 km from the epicenter. **a** Modeling with the focal mechanism solution obtained in this work using Nábelék technique. **b** Results obtained using Yagi *et al.*, (2004) geometry

event, and they enclose the southeast aftershock area of the 9 October 1995 ($M_w = 8.0$) Colima–Jalisco earthquake. The Tecomán earthquake ruptured approximately half of the Colima gap. Most aftershocks occurred inside the subducted slab, and our aftershock locations (Fig. 5) have features similar to those reported by NÚÑEZ-CORNU *et al.*, (2004) and YAGI *et al.*, (2004). For example, they report an elongated trend of aftershocks from southeast to northwest and three clusters of activity; however, their locations have a trend toward the southwest. Our aftershock locations are spread in an extended area close to the seashore with some of the features reported by NÚÑEZ-CORNU *et al.*, (2004) and YAGI *et al.*, (2004).

Source parameters of the Tecomán earthquake were calculated from the spectra of P-waveforms recorded at teleseismic distances. A corner frequency was observed at $f = 0.05 \pm 0.05$ Hz, a stress drop of 5.4 ± 2.5 MPa (54 ± 25 bars) and a seismic moment of $2.7 \pm 0.70 \times 10^{20}$ Nm ($2.7 \pm 0.7 \times 10^{27}$ dynes cm) were calculated assuming that BRUNE's (1970) circular fault model holds. We note the lower stress drop value calculated with teleseismic data compared with that obtained using local and regional records (YAGI *et al.*, 2004, SINGH *et al.*, 2003). This result would imply that Tecomán earthquake was deficient in high-frequency radiation. This, however, appears not to be the case from the reported severe damage to buildings in the localities situated at distances where along-trench rupturing subduction earthquakes of the same magnitude usually do not produce any

significant damage (ZOBIN and PIZANO-SILVA, 2007). We think, therefore, that a low rupture velocity is more likely the cause of the low stress drop value obtained from spectral analysis.

Besides the waveforms used by YAGI *et al.*, (2004) we included, in the inversion of near field body waves, the waveforms recorded at the Manzanillo power plant (MNZ), a strong motion station located 54.0 km from the epicenter. Those body waveform were not used by YAGI *et al.*, (2004). In the inversion process we assumed a rectangular fault area of 70 by 100 km and a depth of the initial break of 25 km. Figure 11 shows a horizontal projection of the fault rupture from our inversion. The slip distribution shows the same asperities reported by YAGI *et al.*, (2004), however, two additional zones of seismic moment release, not so energetic in their inversion, appeared clearly defined in our analysis as a significant zone of seismic moment release up-dip and down-dip. The total source duration was 30 s and a seismic moment of 1.88×10^{20} Nm ($M_w = 7.5$). A significant seismic moment release was observed at the end of the rupture process; this seismic moment released was located down-dip below the Manzanillo seismic station and up-dip. The source time duration of 20 s calculated with the spectra of teleseismic body-waves and with the inversion of P and SH waves using the NÁBELÉK, (1984) method agree with the main source energy release. On the other hand, source time duration obtained with the inversion of teleseismic and near-source strong motion stations is 30 s, however the maximum seismic moment release

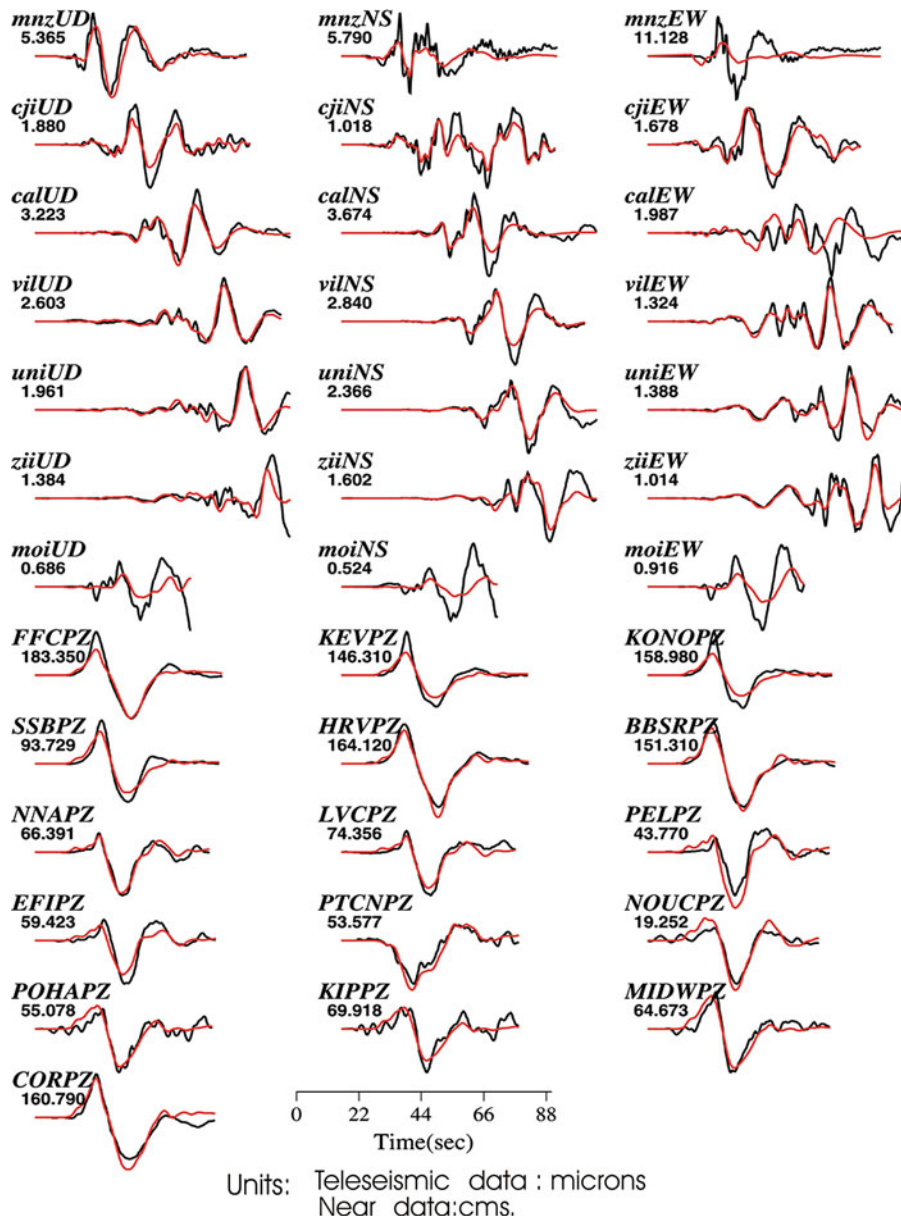


Figure 10

Comparison of the observed waveforms (black line) with the calculated waveforms (red line) obtained from the inversion. Seven upper records correspond to strong motion data of Mexican stations. Six lower seismograms are teleseismic records. Numbers below the station name are the maximum amplitude in centimeters and microns of strong-motion and teleseismic records, respectively

lasted about 20 s (see Fig. 11b). We think that the large source duration obtained with the two dimensional method of inversion is due to the effect of the contribution of energy recorded on the strong-motion (MNZ) stations which was not observed at teleseismic stations.

It is worth mentioning that the uncertainties suggested by BERESNEV, (2003) about the slip inversions using body waves did not have much effect in our study. We did not find great disagreement in the inversion process for the spatial slip distribution. On the other hand, we found an improvement in the

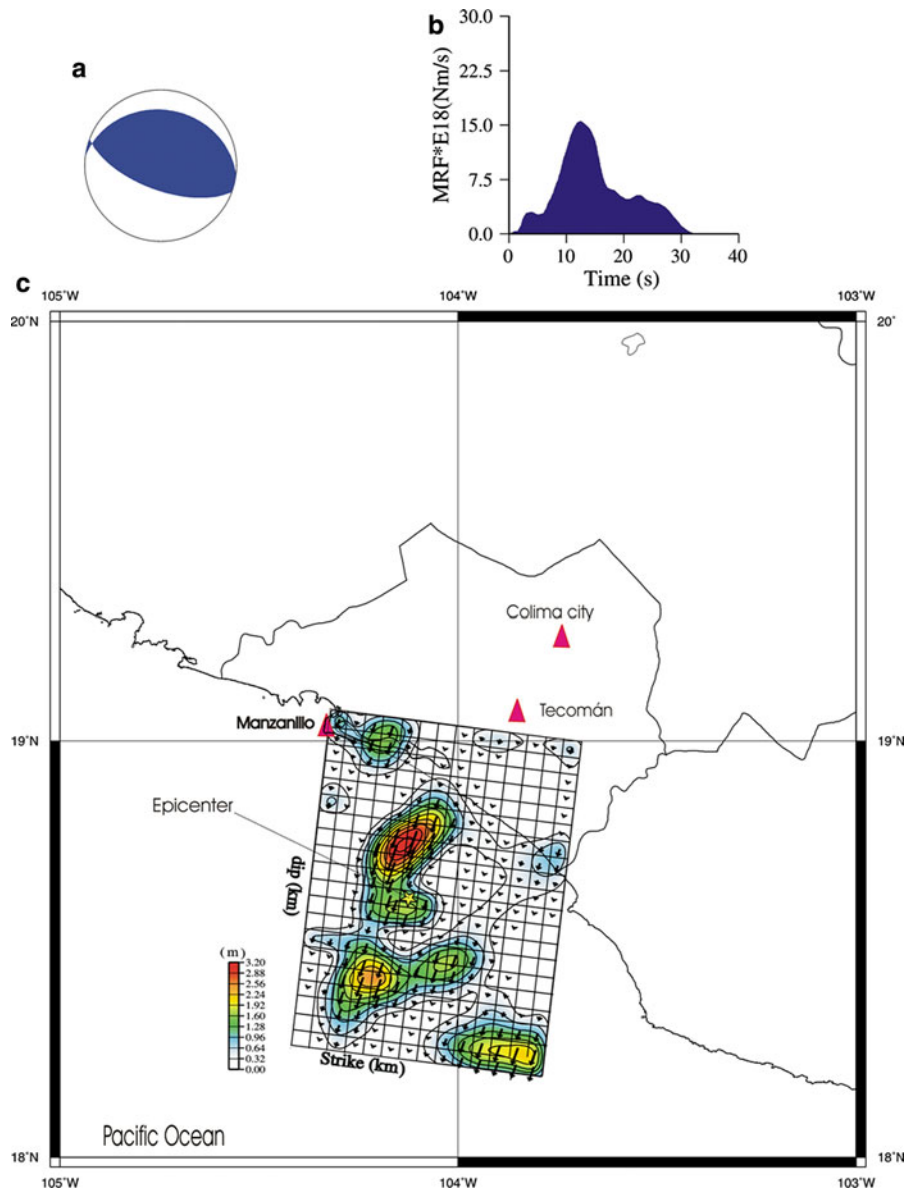


Figure 11

a Fault plane solution used for the slip distribution inversion on the fault plane. **b** Source time function obtained in this inversion. **c** Horizontal projection of the fault showing the slip distribution. Triangle shows the location of the Manzanillo power plant, where it is located the MNZ strong motion recorder, Colima and Tecomán cities

spatial slip distribution by adding the new near source body waveforms into the inversion, therefore, the quality and quantity of waveforms in the near and far field will greatly improve our knowledge of the source process as suggested by IDE *et al.*, (2005).

Acknowledgments

We would like to thank Arturo Pérez-Vertti for the fieldwork and Antonio Mendoza for helping to handle the digital data. Thanks to the following networks for

providing seismic data through the Incorporated Research Institutions for Seismology (IRIS) Data Management Center: FDSN, GEOFON, Geoscope, IDA, GTSN, UI, USGS. We acknowledge El Consejo Nacional de Ciencia y Tecnología (CONACYT) for sponsoring part of this project (Proyecto 37038-T). One of us (HERL) was supported by a scholarship from PROMEP.

REFERENCES

- BERESNEV, I. A. (2003), *Uncertainties in Finite-Fault Slip Inversion: To What Extent to Believe?*, Bull. Seismol. Soc. Am. 93, 2445–2458.
- BEZZEGHOUD, M., DESCHAMPS, A. and MADARIAGA, R., Broad-band P-wave Signals and Spectra from Digital stations. In *Digital Seismology and Fine Modeling of the Lithosphere* (eds. Cassinis, R., Nolet, G., and Panza, G.F.) (Plenum Press, New York, 351–374, 1989).
- BRUNE, J.N. (1970), *Tectonic stress and the spectra of seismic shear waves from earthquakes*, J. Geophys. Res. 75, 4997–5009.
- FUTTERMAN, W.I. (1962), *Dispersive body waves*, J. Geophys. Res. 67, 5279–5291.
- SUÁREZ, G., GARCIA-ACOSTA, V. and GAULON, R. (1994), *Active crustal deformation in the Block, Mexico: evidence for great historical earthquake in the 16th century*, Tectonophysics 234, 117–127.
- HARTZELL, S. H. and HEATON, T.H. (1983), *Inversion of strong ground motion and teleseismic waveform data for the fault rupture history of the 1979 Imperial Valley, California earthquake*, Bull. Seismol. Soc. Am. 73, 1553–1583.
- IDE, S., BEROZA, G.C. and MCGUIRE, J.J., *Imaging earthquake source complexity*, Geophysical Monograph 157, *Seismic earth: Array analysis of broadband seismograms* (eds. Levander, A. and Nolet, G. (American Geophysical Union, Washington, D. C., pp. 2005).
- KIKUCHI, M., and KANAMORI, H. (1991), *Inversion of Complex Body Waves-III*, Bull. Seismol. Soc. Am. 81, 2335–2350.
- KOHKETSU, K. (1985), *The extended reflectivity method for synthetic near-field seismograms*, J. Phys. Earth 33, 121–131.
- KOSTOGLODOV, V., and BANDY, W. (1995), *Seismotectonic constraints on the rate between the Rivera and North American plates*, J. Geophys. Res. 100, 977–990.
- NÁBÉLEK, J. (1984), *Determination of earthquake source parameters from inversion of body waves*, PhD. Thesis (Mass. Inst. of Technol., Cambridge), 346 pp.
- NÚÑEZ-CORNÚ, F. J., REYES-DÁVILA, G.A., RUTZ LÓPEZ, M., TREJO GOMEZ, R., CAMARENA-GARCÍA, M.A. and RAMÍREZ-VAZQUEZ, C.A. (2004), *The 2003 Armeria, Mexico Earthquake ($M_w = 7.4$): Mainshock and early aftershocks*, Seismological Research Letters 75, pp. 506–605.
- PACHECO, J. F., and SYKES, L. (1992), *Seismic moment catalog of large shallow earthquakes, 1900 to 1989*, Bull. Seismol. Soc. Am. 82, 1306–1349.
- PACHECO, J., SINGH, S. K., DOMINGUEZ, J., HURTADO, A., QUINTANAR, L., JIMÉNEZ, Z., YAMAMOTO, J., GUTIÉRREZ, C., SANTOYO, M., BANDY, W., GUZMAN, M., KOSTOGLODOV, V., REYES, G. and RAMÍREZ, C. (1997), *The October 9, 1995 Colima-Jalisco, Mexico earthquake ($M_w 8$): an aftershock study and comparison of this earthquake with those of 1932*, Geophys. Res. Lett. 24, 2223–2226.
- PARDO, M., and SUÁREZ, G. (1995), *Shape of the subducted Rivera and Cocos plates in Southern Mexico: Seismic and tectonic implications*, J. Geophys. Res. 100, 12357–12373.
- REYES, A., BRUNE, J. N. and LOMNITZ, C. (1979), *Source mechanism and aftershock study of the Colima, Mexico earthquake of January 30, 1973*, Bull. Seismol. Soc. Am. 69, 1819–1840.
- SINGH, S.K., PONCE, L. and NISHENKO, S. P. (1985), *The great Jalisco, Mexico, earthquakes of 1932: subduction of the Rivera plate*, Bull. Seismol. Soc. Am. 75, 1301–1313.
- SINGH, S. K., PACHECO, J. F., ALCÁNTARA, L., REYES, G., ORDAZ, M., IGLESIAS, A., ALCOCER, S. M., GUTIERREZ, C., VALDÉS, C., KOSTOGLODOV, V., REYES, C., MIKUMO, T., QUAAS, R., ANDERSON, J.G. (2003), *Contributions. A Preliminary Report on the Tecomán, Mexico Earthquake of 22 January 2003 ($Mw 7.4$) and Its Effects*. Seism. Res. Lett. 74, 279–289.
- YAGI, Y., KIKUCHI, M., YOSHIDA, S. (1999), *Comparison of the coseismic rupture with the aftershock distribution in the Hyuga-nada earthquakes of 1996*, Geophys. Res. Lett. 26, 3161–3164.
- YAGI, Y., MIKUMO, T., PACHECO, J., and REYES, G. (2004), *Source rupture process of Tecomán, Colima, Mexico earthquake of January 22, 2003, determined by joint inversion of teleseismic body-wave and near-source data*, Bull. Seismol. Soc. Am. 94, 1795–1807.
- YOSHIDA, S. (1989), *Waveform inversion using ABIC for the rupture process of the 1983 Hindu-Kush earthquake*, Phys. Earth Planet. Inter. 56, 389–405.
- YOSHIDA, S. (1992), *Waveform inversion for rupture process using a non-flat seafloor model: application to 1986 Andreanof Islands and 1985 Chile earthquakes*, Tectonophysics 211, 45–59.
- ZOBIN, V.M. and PIZANO-SILVA, J.A. (2007), *Macroseismic Study of the $M_w 7.5$ 21 January 2003 Colima, México, Across-Trench Earthquake*, Bull. Seismol. Soc. Am. 97, 1221–1832.

(Received February 11, 2010, revised September 22, 2010, accepted September 23, 2010, Published online November 16, 2010)